Cerebellum (2013) 12:862–869
DOI 10.1007/s12311-013-0499-2

ORIGINAL ARTICLE

Frequency-Dependent Reliability of Spike Propagation Is Function of Axonal Voltage-Gated Sodium Channels in Cerebellar Purkinje Cells

Zhilai Yang · Jin-Hui Wang

Published online: 18 June 2013

Abstract The spike propagation on nerve axons, like synaptic transmission, is essential to ensure neuronal communication. The secure propagation of sequential spikes toward axonal terminals has been challenged in the neurons with a high firing rate, such as cerebellar Purkinje cells. The shortfall of spike propagation makes some digital spikes disappearing at axonal terminals, such that the elucidation of the mechanisms underlying spike propagation reliability is crucial to find the strategy of preventing loss of neuronal codes. As the spike propagation failure is influenced by the membrane potentials, this process is likely caused by altering the functional status of voltage-gated sodium channels (VGSC). We examined this hypothesis in Purkinje cells by using pair-recordings at their somata and axonal blebs in cerebellar slices. The reliability of spike propagation was deteriorated by elevating spike frequency. The frequency-dependent reliability of spike propagation was attenuated by inactivating VGSCs and improved by removing their inactivation. Thus, the functional status of axonal VGSCs influences the reliability of spike propagation.

Keywords Axon · Neuron · Action potential · Spike propagation · Purkinje cell · Cerebellum

Electronic supplementary material The online version of this article (doi:10.1007/s12311-013-0499-2) contains supplementary material, which is available to authorized users.

Z. Yang · J.-H. Wang (✉)
State Key lab for Brain and Cognitive Sciences, Institute of Biophysics, Chinese Academy of Sciences, Beijing 100101, China
e-mail: jhw@sun5.ibp.ac.cn

Z. Yang · J.-H. Wang
University of Chinese Academy of Sciences, Beijing 100049, China

Introduction

The axons as a subcellular compartment of neurons play critical roles in processing neural codes [1, 2], such as the initiation of action potentials [3–13], the amplification of neuronal spikes [14, 15], and the propagation of spikes toward the terminals [16–21]. The patterns of axon-initiated spikes constitute neuronal codes to control brain functions. The amplification of spikes ensures the neuronal codes to be digital in nature. The reliability of spike propagation influences the spikes to be efficient codes in neuronal networks. The study to draw a comprehensive picture for these axonal functions is critically important for understanding the computational processes in the brain.

The secure propagation of sequential spikes toward axonal terminals has been challenged recently [19, 20, 22–24]. The shortfall of spike propagation was often seen in the neurons that fired high-frequency spikes [1, 25], such as cerebellar Purkinje cells whose firing rate were up to 500 Hz [6, 26–28]. This unreliability of spike propagation enables some digital spikes disappear at axonal terminal. In order to secure the spike propagation without losing neuronal digital codes, we have to understand the mechanism underlying their propagation unreliability.

The spike propagation was affected by membrane potentials and axonal branch points [1]. For instance, the reliability of spike propagation was worsen by membrane depolarization and improved by hyperpolarization [20, 24]. Spike propagation was based on a local current that activated voltage-gated sodium channels (VGSC). Membrane potentials affected VGSC kinetics [29–31]. Therefore, the unreliability of spike propagation may result from the changes in VGSC's functional status. We tested this hypothesis in the main axons from cerebellar Purkinje cells, and observed the frequency-dependent unreliability of spike propagation caused by VGSC inactivation.

Methods and Materials

Brain Slices and Neurons All experiments were approved by the Institutional Animal Care Unit Committee in Administration Office of Laboratory Animals Beijing China (B10831). Cerebellar sagittal slices (400 μm) were prepared from Wistar rats in postnatal days (PND) 14~15 under the anesthesia by injecting chloral hydrate (300 mg/kg) for decapitation by a guillotine. Slices were cut by Vibratome in a modified and oxygenized (95 % O_2 and 5 % CO_2) artificial cerebrospinal fluid (millimolar: 124 NaCl, 3 KCl, 1.2 NaH_2PO_4, 26 $NaHCO_3$, 0.5 $CaCl_2$, 5 $MgSO_4$, 10 dextrose, and 5 HEPES; pH 7.4) at 4 °C, and were held in normal oxygenated ACSF (millimolar: 126 NaCl, 2.5 KCl, 1.25 NaH_2PO_4, 26 $NaHCO_3$, 2 $CaCl_2$, 2 $MgSO_4$, and 25 dextrose; pH 7.4) at 35 °C for 1–2 h. A slice was transferred to a submersion chamber (Warner RC-26G) and perfused by normal ACSF for the electrophysiological experiments [14, 32–36].

Cerebellar Purkinje cells were identified based on their morphology and functions. Purkinje cells in the slices for whole-cell recording were located at the border between molecular layer and granule cells (soma above 40 μm), and infused by fluorescence Alex-488 (5 μM in pipettes) under a DIC/fluorescent microscope (Nikon, FN-E600) to show their typical dendrites and guide tracing main axonal terminals for loose-patch recording axon spikes. Purkinje cells were labeled by neurobiotin (Fig. 1a). Purkinje cells showed fast spiking with no adaptation in amplitudes and frequencies [13, 37–40]. The use of this preparation for our study is based on their unique features. Purkinje cells in response to peripheral stimuli in vivo showed that membrane depolarization lasted for long duration from hundreds of milliseconds to seconds [41, 42] and produced high-frequency spikes [6, 26–28].

Electrophysiological Studies Sequential spikes in Purkinje cells propagate on their axons. The experiments were designed

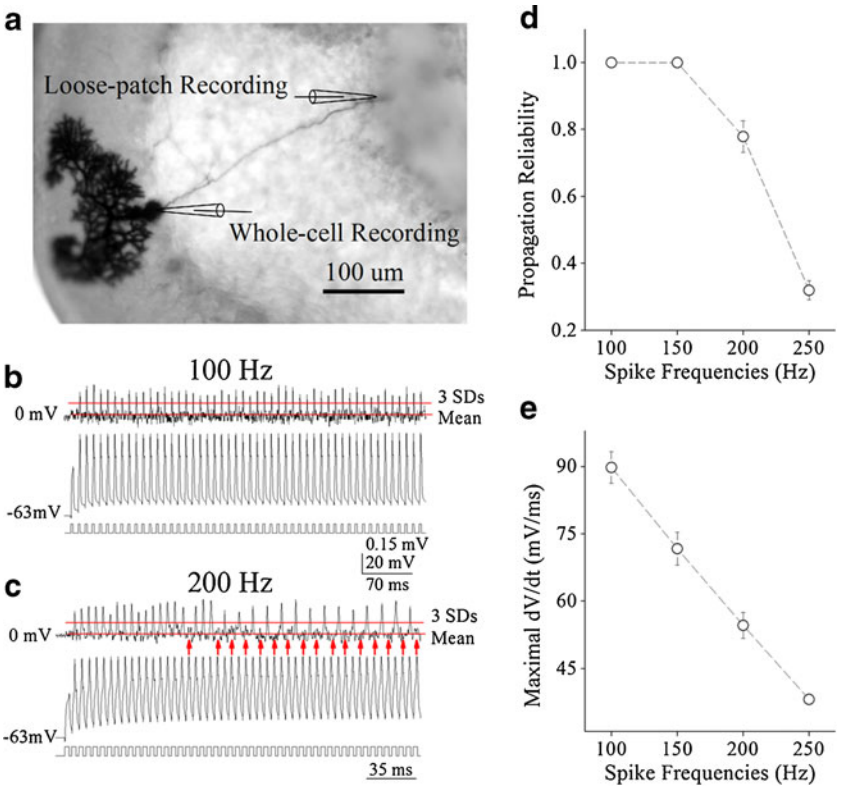

Fig. 1 The reliability of spike propagation on the axons of cerebellar Purkinje cells decreases when spike frequency increases. **a** Diagram of a whole-cell recording on soma and a loose-patch recording on axonal bleb. Cell is a neurobiotin-labeled –Purkinje cell whose main axon extends toward deep cerebellar nucleus (please see "Methods and Materials" section). **b** Top trace illustrates axonal spikes recorded by a loose-patch on axonal bleb and bottom trace shows spikes recorded by a whole-cell pipette at PC soma. The somatic spikes are induced by sequential depolarization pulses at 100 Hz. **c** Top trace illustrates axonal spikes recorded by a loose-patch on axonal bleb and bottom trace shows spikes recorded by a whole-cell pipette at PC soma. Somatic spikes are induced by sequential depolarization pulses at 200 Hz. *Red arrows* under loose-patch recorded signals show the failure of spike propagation on the axons. *Red lines* show mean and standard deviation at three-times of noise. *Calibration bars* are 0.15 mV for loose-patch spikes, 20 mV for whole-cell spikes, 70 ms for **b** and 35 ms for **c**. **d** Somatic spike frequencies versus propagation reliability (a ratio of axonal spikes to somatic ones) on the axons (n=13). **e** Somatic spike frequencies versus spike's maximal dV/dt (n=13)

as whole-cell recordings on their somata and loose-patch recordings on the remote ends of their axonal blebs (Fig. 1a), such that spike propagation on axons was measured. The electrical signals were recorded by MultiClapm-700B amplifier (Axon Instrument Inc., CA, USA) and inputted into pClamp-10 in 50 kHz sampling rate. Transient capacitance was compensated and output bandwidth was 3 kHz. Pipette solution for recording spikes included (millimolar) 150 K-gluconate, 5 NaCl, 0.4 EGTA, 4 Mg-ATP, 0.5 Tris–GTP, 4 Na-phosphocreatine, and 10 HEPES (pH 7.4 adjusted by 2 M KOH). The solution for loose-patch recording was the ACSF. The osmolarity of pipette solutions made freshly was 295–305 mOsmol. Pipette resistance was 8~10 MΩ [43–46].

In studying spike propagation on the axons of Purkinje cells, we injected depolarization pulses in various durations and intervals into their somata to induce spikes at 100~250 Hz. Synchronous spikes at the soma and axonal bleb indicated the signals from a Purkinje cell. The efficiency to propagate spikes on the axons of Purkinje cells was assessed by the ratio of spikes recorded at axonal terminals to those spikes induced on soma, which was defined as spike propagation fidelity. It was noteworthy that the number of induced-spikes was reduced under the condition of high-frequency stimuli, such that spike propagation fidelity or action potential maximal d*V*/d*t* vs. spike frequencies was calculated from the first 50 spikes (Figs. 1d–e, 2c–d, and 3e–f). In addition, the features of spike propagation are given in Fig. S3 (please see "Electronic Supplementary Material").

The influence of VGSC's functional status on spike propagation was studied. The inactivation of VGSCs was prevented by using anemone toxin (ATX), a blocker of VGSC inactivation [47, 48], and using hyperpolarization pulses [30, 37]. Five micromolar ATX was puffed onto the middle segment of axons by ATX-containing pipette, while

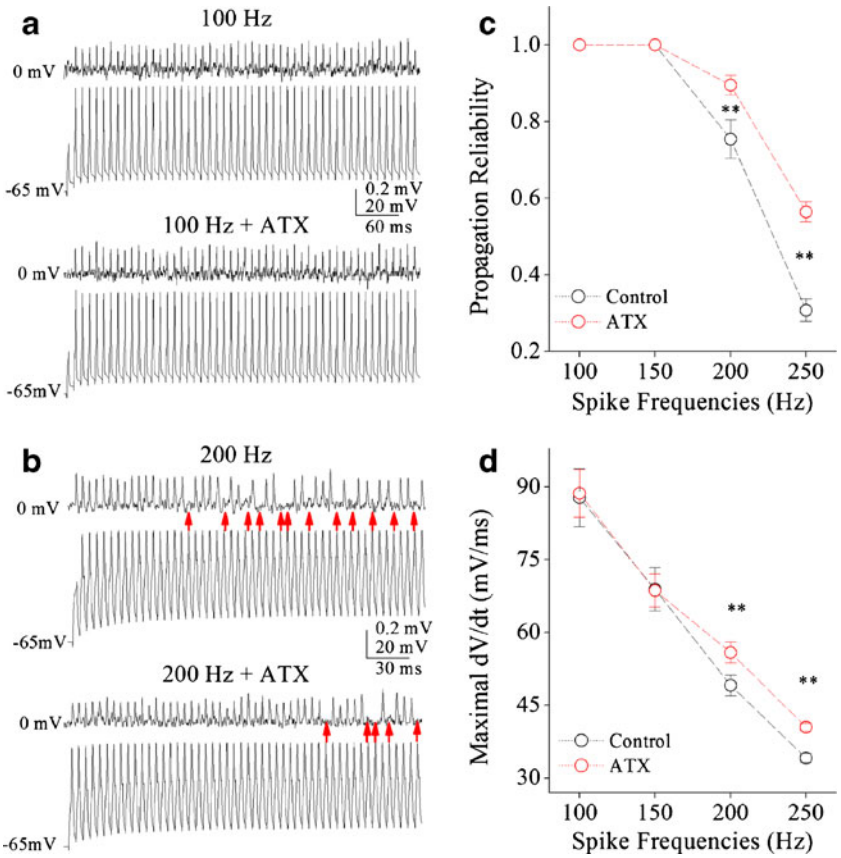

Fig. 2 Anemone toxin (ATX), the blocker of the inactivation of voltage-gated sodium channel (VGSC), improves the frequency-dependent unreliability of spike propagation on the axons of cerebellar Purkinje cells. **a** *Top panel* shows axonal spikes recorded by loose-patch on axonal bleb (*top trace*) and somatic spikes induced by a whole-cell pipette at 100 Hz of depolarization pulses (*bottom trace*) under the control. *Bottom panel* shows axonal spikes (*top trace*) and somatic spikes induced by 100 Hz of depolarization pulses (*bottom trace*) under the condition of 5 μM ATX. **b** *Top panel* shows axonal spikes (*top trace*) and somatic spikes induced by 200 Hz of depolarization pulses (*bottom trace*) under the control. *Bottom panel* shows axonal spikes (*top trace*) and somatic spikes induced by 200 Hz of depolarization pulses (*bottom trace*) under 5 μM ATX. *Red arrows* indicate the failure of spike propagation to axonal terminals. *Calibration bars* are 0.2 mV for loose-patch spikes, 20 mV for whole-cell spikes, 60 ms for **a** and 30 ms for **b**. **c** Somatic spike frequencies vs. propagation reliability (a ratio of axonal spikes to somatic ones) under the conditions of control (*black symbols*) and ATX (*reds*; *two asterisks*, $p<0.01$; $n=9$). **d** Relationship between spike's maximal d*V*/d*t* and spike frequencies under the conditions of control (*black symbols*) and ATX (*reds*; *two asterisks*, $p<0.01$; $n=9$). Axonal length was in a range of 200~350 μm

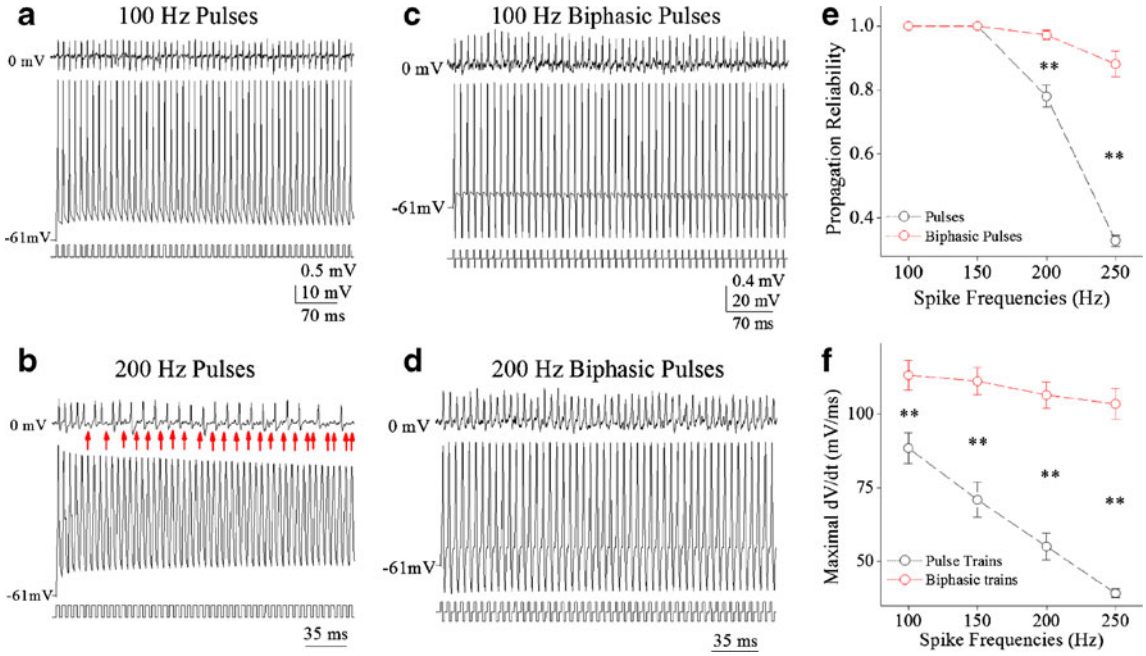

Fig. 3 Afterhyperpolarization (AHP) improves frequency-dependent unreliability of spike propagation on the axons of cerebellar Purkinje cells. **a** Axonal spikes recorded by loose-patch on axonal bleb (*top trace*) and somatic spikes induced by a whole-cell pipette at 100 Hz of depolarization pulses (*bottom*). **b** Axonal spikes (*top trace*) and somatic spikes induced by 200 Hz of depolarization pulses (*bottom*). *Red arrows* indicate the failure of spike propagation to the axonal terminals. Calibration bars are 0.5 mV for loose-patch spikes, 10 mV for whole-cell spikes, 70 ms for **a** and 35 ms for **b**. **c** Axonal spikes (*top trace*) and somatic spikes induced by 100 Hz of biphasic pulses (i.e., depolarization plus hyperpolarization in *bottom trace*). **d** Axonal spikes (*top trace*) and somatic spikes induced by 200 Hz of biphasic pulses (*bottom*). *Calibration bars* are 0.4 mV for loose-patch spikes, 20 mV for whole-cell spikes, 70 ms for **c** and 35 ms for **d**. **e** Somatic spike frequencies versus propagation reliability (a ratio of axonal spikes to somatic ones) under the conditions of control (*black symbols*) and AHP (*reds*; *asterisks*, $p<0.01$; $n=10$). **f** Relationship between spike's maximal dV/dt and spike frequencies under the conditions of control (*black symbols*) and AHP (*reds*; *two asterisks*, $p<0.01$; $n=10$). Axonal length was in a range of 200~350 μm

using whole-cell recording on soma and loose-patch recording on axonal bleb. The strengthened VGSC inactivation was made by using a steady depolarization in 1 s [30, 37]. Spike frequency induced by steady depolarization was calculated based on the number of spikes per second.

The data were analyzed if the recorded neurons had resting membrane potentials negatively more than −60 mV and action potentials above 65 mV. The criteria for the acceptation of each experiment also included less than 5 % changes in resting membrane potential, spike magnitude, input, and seal resistance. The values of spike propagation reliability and action potential maximal dV/dt are presented as mean±SE. As the experiments for different spike frequencies and control vs. various treatments (such as ATX and hyperpolarization) were conducted in the given cells, statistical comparisons were done by paired t test.

Neurobiotin Staining for Cerebellar Cells Pipette solutions for whole-cell recordings included 0.2 % neurobiotin, which was back-filled into the recording pipettes whose tips contained the standard solution. After electrophysiological study, the slices were rapidly placed into 4 % paraformaldehyde in 0.1 M phosphate buffer solution (PBS) for fixation at 4 °C about 48 h. The slices were incubated in avidin and horseradish peroxidase (Vectastain ABC) for 3 h, and then 1 % DAB–CoCl2 (Sigma) 1 min for staining neurobiotin-filled cells. This reaction was stopped by PBS [49]. Neurobiotin-stained cells were photographed under a scanning confocal microscope (Olympus FV-1000, Japan).

Results

In the study of spike propagation reliability, we applied the following strategies. The relationship between spike propagation reliability and spike frequency was analyzed to characterize spike propagation. In terms of the influence of VGSC on spike propagation reliability, we upregulated or downregulated the functional status of VGSCs, and analyzed the changes in the reliability of spike propagation. The correlated changes between VGSC function and spike propagation reliability indicate whether the reliability of spike propagation is under the control of VGSC functional status.

Frequency-Dependent Reliability of Spike Propagation on Axons of Cerebellar Purkinje Cells

In pair-recording on cerebellar Purkinje cells (Fig. 1a), sequential spikes were evoked on their somata and the propagated spikes were recorded at their axonal blebs. The reliability of spike propagation was assessed by a ratio of number of spikes propagated into axonal bleb to that of spikes evoked at soma [19, 20, 25]. The spikes propagated to the axonal blebs were accounted if their amplitudes were above the values of mean plus three-times in standard deviation of axonal noise signals (red lines in Fig. 1b–c; also see [19]).

We first measured the reliability of spike propagation at different spiking frequencies. In Fig. 1b–c, somatic spikes induced by whole-cell recording pipette are showed in bottom traces, and axonal spikes recorded by loose-patch pipette are in top traces. The spikes failed in their propagation are pointed by red arrows. By comparing spike propagation in response to spike frequencies at 100 (Fig. 1b) and 200 Hz (Fig. 1c), we see that some spikes fail to propagate to axonal blebs when spike frequency is 200 Hz. A plot for propagation reliability vs. spike frequencies in Fig. 1d shows that the values of propagation reliability are 1±0, 1±0, 0.79±0.05 and 0.32±0.03 in response to spike frequencies at 100, 150, 200, and 250 Hz, respectively. The reliability of spike propagation is reducing after the spike frequency rises above 150 Hz (n=13). This result supports the frequency-dependent unreliability of spike propagation on the axons of Purkinje cells [19, 20, 23, 24].

The spike propagation on the axons is a process of spike regeneration in a segment-by-segment manner via local currents that activate VGSCs. Sodium channels play critical roles in spike propagation, and their availability is frequency dependent, so that spike frequency is associated to VGSC inactivation. This frequency-dependent propagation unreliability may be caused by VGSC inactivation. We used spike maximal dV/dt to indicate VGSC availability. Figure 1e shows the values of spikes' maximal dV/dt are 89.8±3.54, 71.7±3.65, 54.7±2.92, and 38.2±1.1 in response to spike frequencies at 100, 150, 200, and 250 Hz, respectively.

In brief, spike propagation on the axons of cerebellar Purkinje cells is unreliable, which depends upon the frequency. When cerebellar Purkinje cells produce spikes in high frequency, their axons may not propagate all of them to the axonal terminals. We then studied the mechanisms underlying the frequency-dependent unreliability of spike propagation, based on the proposal that spike propagation was controlled by VGSC's functional status. If it is a case, we expect to see that spike propagation reliability is improved by facilitating VGSC recovery from inactivation and is worsen by inactivating VGSCs.

A Facilitation of VGSC Recovery from Inactivation Improves the Unreliability of Spike Propagation

The facilitation of VGSC recovery from the inactivation was fulfilled by using the approaches of pharmacology and biophysics. In pharmacological study, we applied anemone toxin (ATX), a blocker of VGSC inactivation [47, 48], to facilitate VGSC recovery from inactivation. Five micromolar ATX was puffed onto the middle segment of axons between the soma and axonal blebs of Purkinje cells. VGSC recovery from inactivation was also facilitated by giving hyperpolarization pulse after each spike [30, 37].

Figure 2 illustrates the effect of ATX on frequency-dependent reliability of spike propagation. Comparing panels a and b of Fig. 2, ATX appears to rescue the failure of spike propagation. The statistical analyses in Fig. 2c demonstrate that the values of spike propagation reliability are 1±0, 1±0, 0.75±0.05, and 0.31±0.03 under the control (black symbols), and are 1±0, 1±0, 0.9±0.03, and 0.56±0.03 under ATX use (red symbols) in response to spike frequencies at 100, 150, 200, and 250 Hz, respectively. The values of propagation reliability corresponding to spike frequencies at 200 Hz and above are different significantly under the conditions of control and ATX (two asterisks, p<0.01, paired t test). Moreover, Fig. 2d shows that maximal dV/dt values are 87.8±5.9, 68.9±4.5, 49.1±2.1, and 34.1±0.9 under controls (black symbols), and are 88.7±5.0, 68.6±3.4, 55.9±2.2, and 40.5±0.8 under ATX usage (red symbols). Spike's maximal dV/dt in correspondence of spike frequencies above 200 Hz is significantly different under the conditions of control and ATX (asterisks, p<0.01). Therefore, a reduction of VGSC inactivation rescues the frequency-dependent unreliability of spike propagation on the axons of cerebellar Purkinje cells.

As hyperpolarization pulses improve VGSC activation [30, 37], we further studied the effect of hyperpolarization pulse on the frequency-dependent unreliability of spike propagation. In Fig. 3a–d, hyperpolarization pulses in biphasic pattern appear to rescue the failure of spike propagation. The statistical analyses in Fig. 3e demonstrate that the values of spike propagation reliability are 1±0, 1±0, 0.78±0.03, and 0.33±0.02 under the control (black symbols), and are 1±0, 1±0, 0.97±0.01, and 0.88±0.04 under biphasic pulses (red symbols) in response to spike frequencies at 100, 150, 200, and 250 Hz, respectively. The propagation reliability corresponding to spike frequencies at 200 Hz and above is different under the conditions of control and hyperpolarization (two asterisks, p<0.01). Moreover, Fig. 3f illustrates that spike's maximal dV/dt values are 88.4±5.2, 70.9±5.9, 55.2±4.5, and 39.3±1.5 under control (black symbols), and are 113.1±5.1, 111.1±4.7, 106.4±4.4, and 103.4±5.3 under hyperpolarization (red symbols). Spike's maximal dV/dt values in correspondence with these

four spike frequencies are significantly different under the conditions of control and afterhyperpolarization (AHP; two asterisks, $p<0.01$). Therefore, the attenuation of VGSC inactivation rescues the frequency-dependent unreliability of spike propagation on axons of cerebellar Purkinje cells.

The Steady Depolarization Leads to VGSC Inactivation and Spike Propagation Unreliability

Spike propagation is based on local currents that activate VGSCs, and the depolarization leads to VGSC inactivation [29–31]. If the reliability of spike propagation is under the control of the functional status of VGSCs, long-lasting depolarization will worsen the reliability of spike propagation. Instead of using a train of depolarization pulses to induce spikes, we applied long-lasting depolarization currents (one second) to evoke spikes, and measured the reliability of spike propagation. Figure 4 shows the effect of long-lasting steady depolarization on spike propagation, in which the depolarization in various intensities was injected into Purkinje cells to induce spikes at different frequencies. When spike frequencies rise by increasing input intensities, more spikes fail to be propagated to axonal terminal (Fig. 4a–d). Compared to spike propagation reliability under the condition of depolarization pulses (triangle symbols in Fig. 4e), the steady depolarization pulse reduces the reliability of spike propagation (circles). Figure 4f shows that spike's maximal dV/dt values decrease with the increase of spike frequencies. Thus, steady depolarization currents worsen frequency-dependent unreliability of spike propagation by strengthened VGSC inactivation in cerebellar Purkinje cells.

Discussion

In terms of the frequency-dependent unreliability of spike propagation on the axons of cerebellar Purkinje cells, our study indicates that propagation reliability is correlated to VGSC availability (Fig. 1). This unreliability of spike propagation is improved by reducing VGSC inactivation (Figs. 2 and 3) and worsened by inactivating VGSC (Fig. 4). Thus, the functional status of voltage-gated sodium channels controls the propagation reliability of digital spikes. In addition to supporting the implication that spike propagation toward axonal terminals may fail [19, 23, 24], our data suggest that

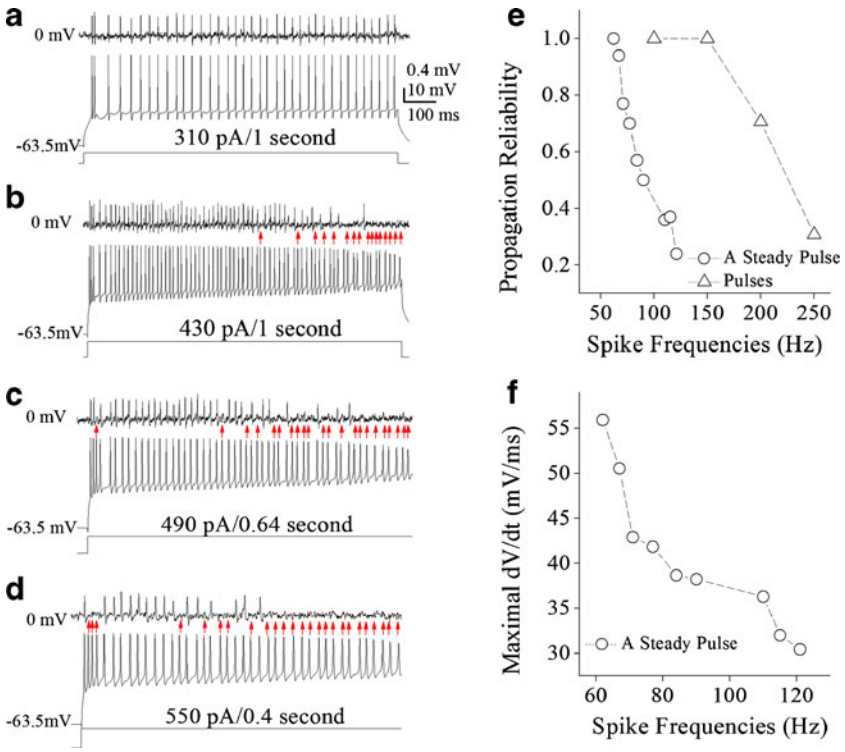

Fig. 4 The steady depolarization worsens the frequency-dependent unreliability of spike propagation on the axons of cerebellar Purkinje cells. **a~d** Axonal spikes recorded by loose-patch on axonal bleb (*top trace*) and somatic spikes induced by a whole-cell pipette at a steady depolarization pulse (*bottom*) in various intensities (310, 430, 490, and 550 pA), which induce somatic spikes with the raised frequency. *Calibration bars* are 0.4 mV for loose-patch spikes, 10 mV for whole-cell spikes and 100 ms for **a** and **b**. **e** Somatic spike frequencies versus propagation reliability (a ratio of axonal spikes to somatic ones) under the conditions of a train of depolarization pulses (*triangle symbols*) and a steady depolarization pulse (*circles*) in various intensities. **f** Spike frequencies versus spike's maximal dV/dt under the conditions of a steady depolarization pulse in various intensities. Axonal length was in a range of 200~350 μm

the effect of membrane potential on spike propagation fidelity [20, 24] is based on the change of VGSC's functional status.

The membrane depolarization recorded in vivo was generally classified into two patterns, a steady depolarization and a fluctuation one [33]. The steady depolarization inactivated VGSCs [29–31, 37]. Hyperpolarization pulses improved VGSC activation [30, 37]. Thus, the spikes generated on the fluctuated pulses are easily propagated toward axonal terminals. In these regards, the reliability of spike propagation is influenced by membrane potentials and input signal patterns, such that the functional status of synapses and cell bodies will regulate spike propagation on the axons, a homeostatic process among subcellular compartments [32].

The studies in cellular imaging suggest that action potentials can reach to axonal terminals. For instance, Ca^{2+} transient was detected at both locations of somatic spike generation and transmitter release [50]. The spikes based on imaging sodium signals indicated that somatic spikes were faithfully propagated toward axon as well as axonal collaterals in the limited frequency (<250 Hz; [51]). The results were obtained from the studies in one spike propagation or proximal axons. This suggestion may not be suitable for sequential spikes and their propagation to axonal terminals. In addition, one could argue that the axons might be injured during cutting cerebellar slices. As the spike propagation infidelity can be almost reversed by afterhyperpolarization to reactivate VGSCs (Fig. 3), this argument may not be an issue.

In general, the location for spike propagation failure is presumably at the first node, branch point and/or entire axon. For instance, TTX application at the first node to block voltage-gated sodium channels attenuates spike propagation reliability [23]. However, the nodes usually contain the highest density of voltage-gated sodium channels [1], such that the first node may not be a site of spike propagation failure. The points of axonal branches in the myelinated axons are often located at the nodes, which contain dense sodium channels. Although the branch points are geometrical factors for spike propagation failure in the unmyelinated axons, it is not a case for the myelinated axons of Purkinje cells in mammalians. In terms of the rest segments of the axons, our results indicate that the spike propagation failure depends upon the inactivation of voltage-gated sodium channels and that the afterhyperpolarization almost reverses spike propagation failure (Fig. 3e). The axonal segments, except for the first node and branch point, are likely involved in spike propagation failure. It is noteworthy that spike propagation reliability does not depend on axonal length since there is no linear correlation between spike propagation reliability and axon length (Fig. S1). In this regard, the location of spike propagation failure remains to be studied by using whole-cell recording and fast imaging along with the entire axons.

The unreliability of spike propagation results from VGSC inactivation ([1, 25] and Figs. 1, 2, 3, and 4), it remains to be studied whether this shortfall of spike propagation is regulated by intracellular signals for its plasticity, which influences the axonal processing of neuronal codes under different conditions. In terms of the physiological impact of spike propagation unreliability, our thoughts include the followings. The precise encoding of the neuronal signals is critical for the brain functions to be homeostatic, which may be maintained by the axonal amplification to spikes [14] and the unreliability of spike propagation (Fig. 1 and [19, 20, 23, 24]). Second, the pathway from cerebellar Purkinje cells to their postsynaptic target cells is inhibitory in nature. The failure of spike propagation in the main axon of Purkinje cells during high frequent spiking prevents their target cells from an over-inhibition via the compatibility between presynaptic and postsynaptic partner [52]. Moreover, to the neurons in the central nervous system, sequential spikes in high-frequency cost much energy and induce seizure. The unreliability of spike propagation plus the failure of synaptic transmission may prevent the energy deficit of the neurons and the seizure of cerebral cortex. In these regards, the optimal points for spike generation and propagation within the efficient and physiological range need to be studied.

Acknowledgments Yang works on experimental analyses. Wang contributes to project design and manuscript writing. This study is supported by the National Basic Research Program (2013CB531304 and 2011CB504405) and Natural Science Foundation China (30990261 and 81171033) to JHW.

Conflict of Interest Authors claim there is no conflict of interest.

References

1. Debanne D, Campanac E, Bialowas A, Carlier E, Alcaraz G. Axon physiology. Physiological Review. 2011;91:555–602.
2. Wu KY, Zhou XP, Luo ZG. Geranylgeranyltransferase I is essential for dendritic development of cerebellar Purkinje cells. Mol Brain. 2010;3:18.
3. Clark BA, Monsivais P, Branco T, London M, Hausser M. The site of action potential initiation in cerebellar Purkinje neurons. Nat Neurosci. 2005;8:137–9.
4. Colbert CM, Pan E. Ion channel properties underlying axonal action potential initiation in pyramidal neurons. Nat Neurosci. 2002;5:533–8.
5. Coombs JS, Curtis DR, Eccles JC. The interpretation of spike potentials of motoneurones. J Physiol Lond. 1957;139:198–231.
6. Davie JT, Clark BA, Hausser M. The origin of the complex spike in cerebellar Purkinje cells. J Neurosci. 2008;28:7599–609.
7. Fuortes MGF, Frank K, Becker MC. Steps in the production of motor neuron spikes. J Gen Physiol. 1957;40:735–52.
8. Hausser M, Stuart G, Racca C, Sakmann B. Axonal initiation and active dendritic propagation of action potentials in substantia nigra neurons. Neuron. 1995;15:637–47.
9. Hu W, Tian C, Li T, Yang P, Hou H, Shu YS. Distinct contribution of Nav1.6 and Nav1.2 in action potential initiation and backpropagation. Nat Neurosci. 2009;12:996–1002.

10. Kole MHP, Ilschner SU, Kampa BM, Williams SR, Ruben PC, Stuart GJ. Action potential generation requires a high sodium channel density in the axon initial segment. Nat Neurosci. 2008;11:178–86.
11. Kuba H, Ishii TM, Ohmori H. Axonal site of spike initiation enhances auditory coincidence detection. Nature. 2006;444:1069–72.
12. Meeks JP, Mennerick S. Action potential initiation and propagation in CA3 pyramidal axons. J Neurophysiol. 2007;97:3460–72.
13. Palmer LM, Clark BA, Grundemann J, Roth A, Stuart GJ, Hausser M. Initiation of simple and complex spikes in cerebellar Purkinje cells. J Physiol Lond. 2010;588:1709–17.
14. Chen N, Yu J, Qian H, Ge R, Wang JH. Axons amplify somatic incomplete spikes into uniform amplitudes in mouse cortical pyramidal neurons. PLoS One. 2010;5(7):e11868.
15. Engel D, Jonas P. Presynaptic action potential amplification by voltage-gated Na+ channels in hippocampal mossy fiber boutons. Neuron. 2005;45:405–17.
16. Chakrabarti L, Eng J, Ivanov N, Garden GA, La Spada AR. Autophagy activation and enhanced mitophagy characterize the Purkinje cells of pcd mice prior to neuronal death. Mol Brain. 2009;2:24.
17. Hodgkin AL, Huxley AF. Propagation of electrical signals along giant nerve fibers. Proc R Soc Lond B Biol Sci. 1952;140:177–83.
18. Huxley AF, Stampfli R. Evidence for saltatory conduction in peripheral myelinated nerve fibres. J Physiol Lond. 1949;108:315–39.
19. Khaliq ZM, Raman IM. Axonal propagation of simple and complex spikes in cerebellar Purkinje neurons. J Neurosci. 2005;25:454–63.
20. Monsivais P, Clark BA, Roth A, Hausser M. Determinants of action potential propagation in cerebellar Purkinje cell axons. J Neurosci. 2005;25:464–72.
21. Stuart G, Spruston N, Sakmann B, Hausser M. Action potential initiation and backpropagation in neurons of the mammalian CNS. Trends Neurosci. 1997;20:125–31.
22. Debanne D, Guerineau NC, Gahwiler BH, Thompson SM. Action-potential propagation gated by an axonal I(A)-like K+ conductance in hippocampus. Nature. 1997;389:286–9.
23. Khaliq ZM, Raman IM. Relative contributions of axonal and somatic Na channels to action potential initiation in cerebellar Purkinje neurons. J Neurosci. 2006;26:1935–44.
24. Meeks JP, Mennerick S. Selective effects of potassium elevations on glutamate signaling and action potential conduction in hippocampus. J Neurosci. 2004;24:197–206.
25. Debanne D. Information processing in the axon. Nat Rev Neurosci. 2004;5:304–16.
26. Eccles JC, Sasaki K, Strata P. Interpretation of the potential fields generated in the cerebellar cortex by a mossy fibre volley. Exp Brain Res. 1967;3:58–80.
27. Harvey RJ, Porter R, Rawson JA. The natural discharges of Purkinje cells in paravermal regions of lobules V and VI of the monkey's cerebellum. J Physiol Lond. 1977;271:515–36.
28. Llinas R, Sugimori M. Electrophysiological properties of in vitro Purkinje cell somata in mammalian cerebellar slices. J Physiol Lond. 1980;305:171–95.
29. Aldrich RW, Corey DP, Stevens CF. A reinterpretation of mammalian sodium channel gating based on single channel recording. Nature. 1983;306:436–41.
30. Chen N, Chen X, Yu J, Wang J-H. After-hyperpolarization improves spike programming through lowering threshold potentials and refractory periods mediated by voltage-gated sodium channels. Biochem Biophys Res Commun. 2006;346:938–45.
31. Goldman L. Stationarity of sodium channel gating kinetics in excised patches from neuroblastoma N1E 115. Biophys J. 1995; 69:2364–8.
32. Chen N, Chen X, Wang J-H. Homeostasis established by coordination of subcellular compartment plasticity improves spike encoding. J Cell Sci. 2008;121:2961–71.
33. Ge R, Qian H, Wang JH. Physiological synaptic signals initiate sequential spikes at soma of cortical pyramidal neurons. Mol Brain. 2011;4:19.
34. Wang J-H. Short-term cerebral ischemia causes the dysfunction of interneurons and more excitation of pyramidal neurons. Brain Res Bull. 2003;60:53–8.
35. Yu J, Qian H, Wang JH. Upregulation of transmitter release probability improves a conversion of synaptic analogue signals into neuronal digital spikes. Mol Brain. 2012;5:26.
36. Zhang F, Liu B, Lei Z, Wang J. mGluR1,5 activation improves network asynchrony and GABAergic synapse attenuation in the amygdala: implication for anxiety-like behavior in DBA/2 mice. Mol Brain. 2012;5:20.
37. Chen N, Zhu Y, Gao X, Guan S, Wang J-H. Sodium channel-mediated intrinsic mechanisms underlying the differences of spike programming among GABAergic neurons. Biochem Biophys Res Commun. 2006;346:281–7.
38. Hockberger PE, Tseng H-Y, Connor JA. Development of rat cerebellar Purkinje cells: electrophysiological properties following acute isolation and in long-term culture. J Neurosci. 1989; 9:2258–71.
39. McKay BE, Turner RW. Physiological and morphological development of the rat cerebellar Purkinje cell. J Physiol Lond. 2005;567:829–50.
40. Qi Y et al. Intracellular Ca2+ regulates spike encoding at cortical GABAergic neurons and cerebellar Purkinje cells differently. Biochem Biophys Res Commun. 2009;381:129–33.
41. Jaeger D, Bower JM. Prolonged responses in rat cerebellar Purkinje cells following activation of the granule cell layer: an intracellular in vitro and in vivo investigation. Exp Brain Res. 1994;100:200–14.
42. Loewenstein Y, Mahon S, Chadderton P, Kitamura K, Sompolinsky H, Yarom Y, et al. Bistability of cerebellar Purkinje cells modulated by sensory stimulation. Nat Neurosci. 2005;8:202–11.
43. Wang JH, Wei J, Chen X, Yu J, Chen N, Shi J. The gain and fidelity of transmission patterns at cortical excitatory unitary synapses improve spike encoding. J Cell Sci. 2008;121:2951–60.
44. Yu J, Qian H, Chen N, Wang JH. Quantal glutamate release is essential for reliable neuronal encodings in cerebral networks. PLoS One. 2011;6:e25219.
45. Zhang G, Gao Z, Guan S, Zhu Y, Wang JH. Upregulation of excitatory neurons and downregulation of inhibitory neurons in barrel cortex are associated with loss of whisker inputs. Mol Brain. 2013;6:2.
46. Zhao J, Wang D, Wang J-H. Barrel cortical neurons and astrocytes coordinately respond to an increased whisker stimulus frequency. Mol Brain. 2012;5(1):10.
47. Mantegazza M, Franceschetti S, Avanzini G. Anemone toxin (ATX II)-induced increase in persistent sodium current: effects on the firing properties of rat neocortical pyramidal neurones. J Physiol Lond. 1998;507(Pt 1):105–16.
48. Rathmayer W. Anemone toxin discriminates between ionic channels for receptor potential and for action potential production in a sensory neuron. Neurosci Lett. 1979;13:313–8.
49. Wang J-H, Kelly PT. Ca2+/CaM signalling pathway up-regulates glutamatergic synaptic function in non-pyramidal fast-spiking neurons of hippocampal CA1. J Physiol Lond. 2001;533:407–22.
50. Mackenzie PJ, Umemiya M, Murphy TH. Ca2+ imaging of CNS axons in culture indicates reliable coupling between single action potentials and distal functional release sites. Neuron. 1996;16:783–95.
51. Foust A, Popovic M, Zecevic D, McCormick DA. Action potentials initiate in the axon initial segment and propagate through axon collaterals reliably in cerebellar Purkinje neurons. J Neurosci. 2010;30:6891–902.
52. Wang JH, Yang Z, Qian H, Chen N. Functional compatibility between Purkinje cell axon branches and their target neurons in the cerebellum. Biophys J. 2013;104:330a.